Cargo Transportation with High Moment of Inertia Payload using T^3-Multirotor

(Abstract) In this paper, we introduce a new freight transportation method based on the T^3-multirotor which is capable of stable transportation of cargoes with a large moment of inertia. The T^3-multirotor, which consists of the 'Thrust Generating Part' and the 'Fuselage Part', can directly control the relative attitude between the two parts using the novel servomechanism. By utilizing the relative attitude control algorithm proposed in this paper, the T^3-multirotor with cargo attached to the fuselage part can maintain constant flight performance regardless of the type of cargo while maintaining system stability during the entire flight. Detailed control methodology, hardware description, and analysis of the dynamic characteristics of T^3-Multirotor with relative attitude control for stable cargo transportation are shown in this paper. The stable cargo flight capacity of the proposed control strategy is validated through experimental results with analysis.

1. INTRODUCTION

The multi-rotor unmanned aerial vehicle is a suitable platform for aerial cargo transportation because of its simple mechanical structure and the operation principle, their ability to fly at a wide range of target flight speeds including hovering flights, and freedom of access to three-dimensional space. However, the flight characteristics of the multirotor may vary considerably depending on the physical characteristics of the attached cargo. When the cargo is too heavy, the available overall thrust force of the platform may not be sufficient to generate enough attitude control torque and total thrust for stable flight. Even when the cargo is not heavy, the stable attitude control may not be secured in case of a cargo having a very large moment of inertia (MOI) such as a long rod. In cases of a heavy-weighted cargo, it is almost the only way to replace the platform with the one that can generate enough thrust. However, in cases of a lightweight cargo but having a large MOI, then stable cargo transportation is possible through the method called as 'Sling-Load Transportation [1]' that transports the cargo by connecting the cargo and the fuselage through the tether.

Sling-load transportation is a commonly used technology for cargo transportation of rotary-wing aircraft. The characteristics that only the tension is exchanged while disconnecting the torque exchange between the cargo and the aircraft fuselage allows the aerial vehicle to maintain attitude control performance compared with the cargo firmly attached to the fuselage since the aerial vehicle does not need to generate additional attitude-controlling torque to rotate the cargo during control. However, sling-load transportation can cause hazardous oscillations similar to pendulum motion [1] and therefore requires an independent algorithm to stabilize the swing angle between the fuselage and the cargo [1], [2]. Also, the sling-load transportation method has the additional disadvantage that it does not control the attitude of the cargo.

As an alternative to sling-load transportation, in this paper, we introduce a new cargo transportation method using T^3-Multirotor [3], a recently developed new type of multi-rotor platform. The T^3-Multirotor platform, originally developed to overcome the underactuatedness of the multi-rotor, consists of a 'Thrust Generating Part' (TGP) with a small mass and moment of inertia (MOI) and a 'Fuselage Part' (FP) with the remaining components (e.g. batteries, sensors, flight computers) required for flight. The TGP and FP are connected through a universal joint mechanism, with a unique servomechanism between the two parts. Through the appropriate relative attitude control (RAC) between two parts via the servomechanism, the T^3-Multirotor can exhibit constant attitude control performance regardless of cargo type as ordinary sling load transportation but free from the oscillation problem.

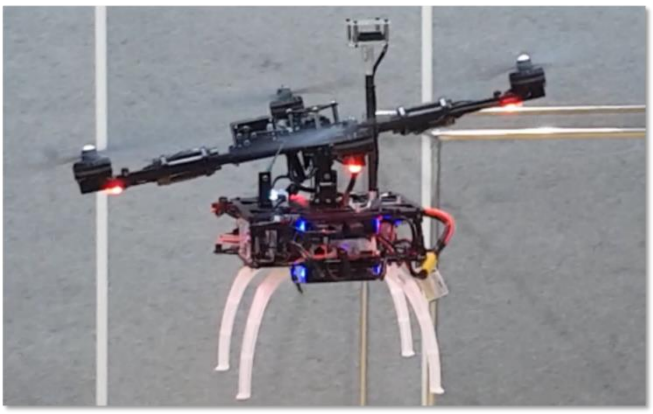

Figure 1. The T^3-Multirotor is capable of direct relative attitude control via the unique servomechanism compared to the sling-rod transport.

This paper is organized as follows. In Section 2, we introduce the new version of T^3-Multirotor hardware, which has been improved over the pervious version [3]. Section 3 presents the mathematical model of the T^3-Multirotor used in the controller design, and Section 4 describes a control strategy to maneuver the T^3-Multirotor when a heavy or large-MOI cargo is attached to the FP. In Section 5, we demonstrate the empirical validity of the proposed theory through actual experiments.

2. HARDWARE DESIGN

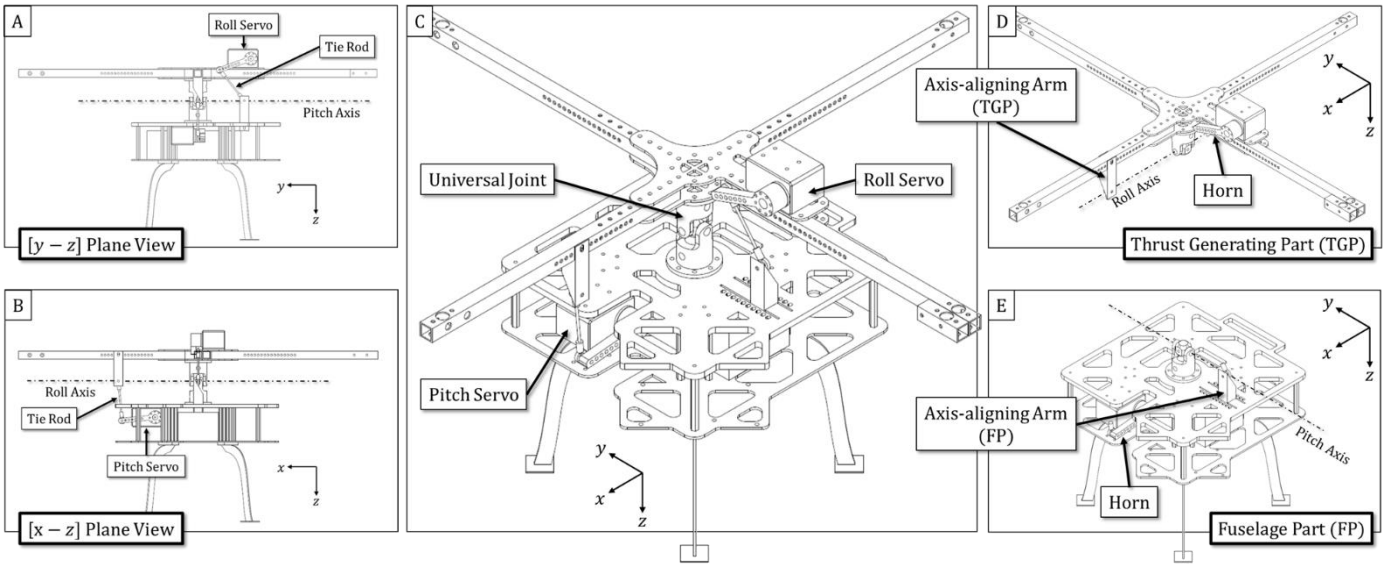

Figure 2. Structure of T^3-Multirotor. The roll and pitch servos independently control the relative roll and pitch attitude between the TGP and FP.

The structure of the T^3-Multirotor used in this study is shown in **Figure 2**. As mentioned earlier, the T^3-Multirotor consists of TGP and FP, which are connected via a universal joint mechanism. From **Figure 2-D**, we can find that the roll axis (x-axis) of the universal joint is always fixed to the TGP frame, regardless of the relative motion between TGP and FP due to the inherent nature of the universal joint. Likewise, the pitch axis (y-axis) of the universal joint is fixed to the FP regardless of the relative motion, as can be seen in **Figure 2-E**. The relative motion is controlled by the servomechanism with roll and pitch servos. The roll servo is attached to TGP, and pitch servo is attached to FP.

A. Servomechanism for Relative Attitude Control between TGP and FP

Figure 3 depicts the roll and pitch servomechanisms. In the case of roll servomechanism, relative roll angle θ_{rr} is controlled by a roll servo angle θ_{rs}. Similarly, relative pitch angle θ_{rp} is controlled by a pitch servo angle θ_{ps} in the case of pitch servomechanism. Point O_{uc} represents the center of the universal joint, and points O_{rs} and O_{ps} represent the rotation center of each servo motors. Points O_{rl} and O_{pu} are located on a structure named as `Axis-aligning arm' (A-arm), and points O_{ru} and O_{pl} are located on a horn of the servo motors. Tie rods are attached between O_{ru} and O_{rl}, and between O_{pu} and O_{pl} to fix the distance between each two points to r_{rr} and r_{pr}, respectively. With A-arm, we can always place points O_{rl} and O_{pu} on the universal joint axis. This leads to the creation of virtual arms $\overline{O_{uc}O_{rl}}$ and $\overline{O_{uc}O_{pu}}$ with lengths of r_{fa} and r_{ta}, where the virtual arm and the relative attitude axis of the opposite servomechanism are always aligned. With this feature, the proposed kinematic structure allows each servo mechanism to operate independently of each other.

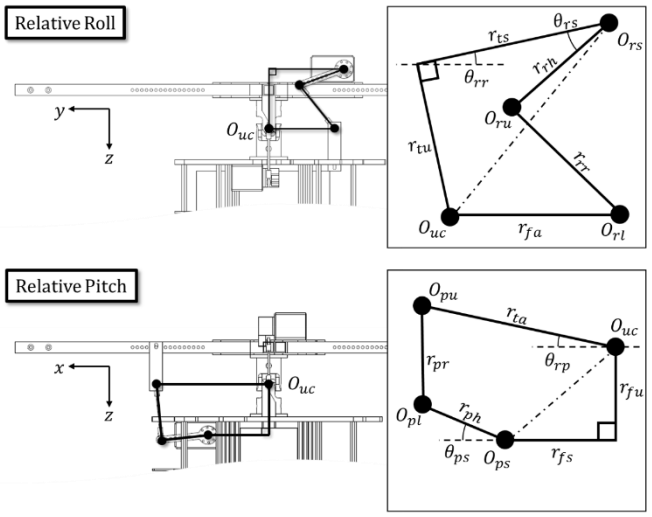

Figure 3. Structure of servomechanism for relative roll and pitch control.

B. Relationship between Servo Angles and Relative Attitude

Since the position of the O_{rs} seen in O_{uc} and O_{ps} seen in O_{uc} are fixed, the servomechanism becomes a general 4-bar linkage system consisting of $\{O_{uc},\ O_{rs},\ O_{ru},\ O_{rl}\}$ and $\{O_{uc},\ O_{ps}, O_{pl},\ O_{pu}\}$. Then, the relationship between servo angle $\theta_{rs},\ \theta_{ps}$, and relative attitude $\theta_{rr},\ \theta_{rp}$ becomes as

$$\begin{cases} \theta_{\text{or}} = f_r(\theta_{rs}) \\ \theta_{rp} = f_p(\theta_{ps}) \end{cases} \tag{1}$$

(refer appendix for detailed f_r and f_p). Using equation (1), we can obtain the required servo angles $\theta_{rs} = f_r^{-1}(\theta_{rr})$ and $\theta_{ps} = f_p^{-1}(\theta_{rp})$ to satisfy the desired $\theta_{rr},\ \theta_{rp}$.

3. MODELLING

During the flight, the TGP and FP of the T^3-Multirotor exchange force and torque through a universal joint. However, the roll and pitch torque among the three-dimensional torque vector components are not exchanged due to the structural characteristics of the universal joint. Instead, roll and pitch torques are generated through servomechanisms. In this section, we cover the equation of motion of the T^3-Multirotor including the roll and pitch torques generated by the servomechanism.

A. General Equations of Motion of TGP and FP

Figure 4 shows the universal joint mechanism and the center of mass (COM) of TGP and FP. Based on the conventional multi-rotor dynamics [8], we can derive the equation of motion of TGP and FP as

$$\begin{cases} m_T\ddot{\mathbf{X}}_T = R(\mathbf{q}_T)\mathbf{F}_T + m_T\mathbf{g} + \mathbf{F}_{F\to T} \\ m_F\ddot{\mathbf{X}}_F = m_F\mathbf{g} + \mathbf{F}_{T\to F} \end{cases} \tag{2}$$

and

$$\begin{cases} J_T\dot{\boldsymbol{\Omega}}_T = \mathbf{T}_T - \boldsymbol{\Omega}_T \times J_T\boldsymbol{\Omega}_T + \mathbf{r}_T \times (R^{-1}(\mathbf{q}_T)\mathbf{F}_{F\to T}) + \mathbf{T}_{F\to T} \\ J_F\dot{\boldsymbol{\Omega}}_F = -\boldsymbol{\Omega}_F \times J_F\boldsymbol{\Omega}_F + \mathbf{r}_F \times (R^{-1}(\mathbf{q}_F)\mathbf{F}_{T\to F}) + \mathbf{T}_{T\to F} \end{cases} \tag{3}$$

where $m_* \in \mathbb{R}$ is the mass, $\mathbf{X}_* = [x_*\ y_*\ z_*]^T \in \mathbb{R}^{3\times1}$ is the position vector, $\mathbf{q}_* = [\phi_*\ \theta_*\ \psi_*]^T \in \mathbb{R}^{3\times1}$ is an attitude vector, $\mathrm{R}(\mathbf{q}_*) \in \mathbb{R}^{3\times3}$ is the rotation matrix from the body frame to earth-fixed frame, $\mathbf{F}_\mathrm{T} = [0\ 0\ -F_T]^T \in \mathbb{R}^{3\times1}$ is the thrust force generated by the set of propellers placed on the TGP, $\mathbf{g} = [0\ 0\ g]^\mathrm{T} \in \mathbb{R}^{3\times1}$ is the gravitational acceleration vector, and $\mathbf{F}_{a\to b} \in \mathbb{R}^{3\times1}$ is the reaction force acting from object *a* to *b*. The parameter $J_* = diag(J_{1,*}, J_{2,*}, J_{3,*}) \in \mathbb{R}^{3\times3}$ is the moment of inertia of the object, $\boldsymbol{\Omega}_* = [p_*\ q_*\ r_*]^T \in \mathbb{R}^{3\times1}$ is the angular velocity vector defined in the body frame, $\mathbf{T}_T = \left[\tau_{r,T}\ \tau_{p,T}, \tau_{y,T}\right]^T \in \mathbb{R}^{3\times1}$ is the torque vector generated by the set of propellers attached to the TGP, $\mathbf{r}_* \in \mathbb{R}^{3\times1}$ is the distance vector from the COM to the center of the universal joint defined in the body frame, and $\mathbf{T}_{a\to b} \in \mathbb{R}^{3\times1}$ is the reaction torque vector acting from object *a* to *b*. The symbol $(*)_T$ and $(*)_\mathrm{F}$ represent TGP and FP respectively. The internal forces and torques acting on the universal joint and servomechanisms follow the additional relationship by the law of action and reaction as

$$\begin{cases} \mathbf{F}_{T\to F} + \mathbf{F}_{F\to T} = 0 \\ R(\mathbf{q}_F)\mathbf{T}_{T\to F} + R(\mathbf{q}_T)\mathbf{T}_{F\to T} = 0. \end{cases} \tag{4}$$

Due to the universal joint mechanism, the following relationship holds between the position vectors $\mathbf{X}_\mathrm{T}$ and $\mathbf{X}_\mathrm{F}$.

$$\mathbf{X}_\mathrm{F} = \mathbf{X}_T + R(\mathbf{q}_T)\mathbf{r}_T - R(\mathbf{q}_F)\mathbf{r}_F \tag{5}$$

B. Translational Motion Equation

From equations (2) and (4), we can obtain the following equation

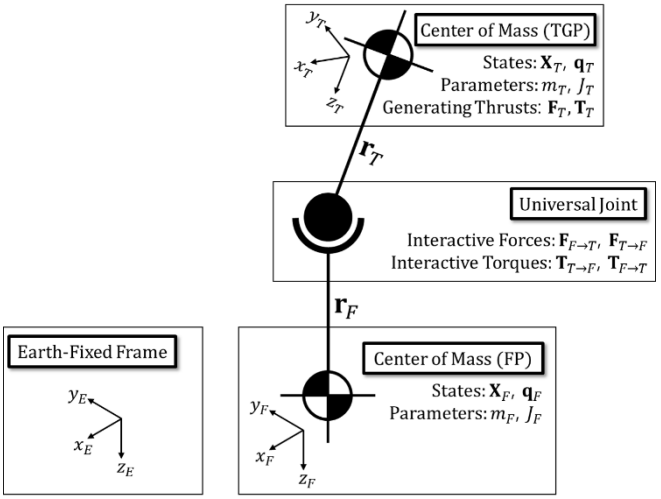

Figure 4. A simplified diagram to overview the relationship between TGP, FP, and universal joint.

$$\mathrm{m}_\mathrm{T}\ddot{\mathbf{X}}_T + m_F\ddot{\mathbf{X}}_F = R(\mathbf{q}_T)\mathbf{F}_T + M\mathbf{g}, \tag{6}$$

where $M = m_T + m_F$. If we set

$$\ddot{\mathbf{X}}_F = \ddot{\mathbf{X}}_T + \Delta_a, \tag{7}$$

where Δ_a is the gap between the acceleration vector of TGP and FP, the translational equations of motion of TGP and FP become as follows.

$$\begin{cases} m_T\ddot{\mathbf{X}}_T = \left(\frac{m_T}{M}\right)R(\mathbf{q}_T)\mathbf{F}_T + m_T\mathbf{g} - \left(\frac{m_Tm_F}{M}\right)\Delta_a \\ m_F\ddot{\mathbf{X}}_F = \left(\frac{m_F}{M}\right)R(\mathbf{q}_T)\mathbf{F}_T + m_F\mathbf{g} + \left(\frac{m_Tm_F}{M}\right)\Delta_a \end{cases} \tag{8}$$

C. Rotational Motion Equation

Through the comparison of equation (2) and (8), we can obtain the internal force of a universal joint as follows

$$\mathbf{F}_{F\to T} = -\left(\frac{m_F}{M}\right)R(\mathbf{q}_T)\mathbf{F}_T - \left(\frac{m_Tm_F}{M}\right)\Delta_a \tag{9}$$

where the value of Δ_a can be obtained from equation (5) and (7). However, we can assume that $\Delta_a \approx 0$ in our case where $\mathbf{q}_T$ and $\mathbf{q}_F$ are controlled within a limited range. Applying equation (9) to (3) with the assumption, the general rotational equations of motion of TGP and FP become

$$\begin{cases} J_T\ddot{\mathbf{q}}_T = \mathbf{T}_T + \mathbf{T}_{F\to T} \\ J_F\ddot{\mathbf{q}}_F = \left(\frac{m_F}{M}\right)\left(\mathbf{r}_F \times (R^{-1}(\mathbf{q}_F)R(\mathbf{q}_T)\mathbf{F}_T)\right) + \mathbf{T}_{T\to F}, \end{cases} \tag{10}$$

where we applied the assumptions $\dot{\boldsymbol{\Omega}} \approx \ddot{\mathbf{q}}$ and $\boldsymbol{\Omega} \times J\boldsymbol{\Omega} \approx 0$ that are widely used in the simplification process of rotational dynamics of the multi-rotors [8].

Now, let us examine the values of $\mathbf{T}_{F\to T}$ and $\mathbf{T}_{T\to F}$ determined by the relative attitude control torque generated by the servomechanism. Thanks to the unique design of the T^3 -Multirotor, the roll servomechanism generates the relative attitude control torque only in the direction of the 'Roll Axis' in **Figure 2-D**, and the pitch servomechanism only in the 'Pitch Axis' in **Figure 2-E**. Since $\mathbf{T}_{F\to T}$ is a value defined based on the body-fixed frame of TGP and

$\mathbf{T}_{T\to F}$ is defined based on the body-fixed frame of FP, $\mathbf{T}_{F\to T}$ and $\mathbf{T}_{T\to F}$ are described as follows

$$\begin{cases}\mathbf{T}_{F\to T} = [\tau_{s,r}\ 0\ 0]^T + R^{-1}(\mathbf{q}_T)R(\mathbf{q}_F)[0\ -\tau_{s,p}\ 0]^T \\ \mathbf{T}_{T\to F} = R^{-1}(\mathbf{q}_F)R(\mathbf{q}_T)[-\tau_{s,r}\ 0\ 0]^T + [0\ \tau_{s,p}\ 0]^T,\end{cases} \quad (11)$$

where $\tau_{s,r} \in \mathbb{R}$ and $\tau_{s,p}\mathbb{R}$ are the roll and pitch servo torques of the servomechanism defined by the body-fixed frame of TGP and FP, respectively. Through equations (10) and (11), we can obtain the following equations.

$$\begin{cases} J_T\ddot{\mathbf{q}}_T = \mathbf{T}_T + \begin{bmatrix}\tau_{s,r}\\0\\0\end{bmatrix} - \begin{bmatrix} -s\theta_{rp}s\phi_F \\ c\phi_F c\phi_T + c\theta_{rp}s\phi_F s\phi_T \\ c\theta_{rp}c\phi_T s\phi_F - c\phi_F s\phi_T\end{bmatrix}\tau_{s,p} \\ J_F\ddot{\mathbf{q}}_F = \left(\frac{m_F r_F F_T}{M}\right)\begin{bmatrix} s\phi_T \\ c\phi_T s\theta_T \\ 0\end{bmatrix} - \begin{bmatrix} c\theta_{rp} \\ -s\theta_{rp}s\phi_F \\ -s\theta_{rp}c\phi_F\end{bmatrix}\tau_{s,r} + \begin{bmatrix}0\\\tau_{s,p}\\0\end{bmatrix}\end{cases} \quad (12)$$

4. CONTROLLER DESIGN

In this section, we illustrate how to maintain the attitude of FP stably while ensuring uniform attitude control performance of the TGP regardless of the type of cargo attached to the FP.

In the case of conventional sling load transportation, the value of $\mathbf{T}_{F\to T}$ in the rotational dynamics of TGP in equation (10) is kept at zero (no servo torque applied), making the TGP behave as a multi-rotor with an MOI of only J_T. However, since $\mathbf{T}_{T\to F}$ must also be zero according to the equation (4), the sole attitude control input of the FP disappears as can be seen from the attitude dynamics of FP in equation (10). As a result, the magnitude of Δ_a of equations (7), (8) and (9) can continuously and rapidly be changed with a large amount due to uncontrolled oscillation, which may lead to a decrease in the translational acceleration control performance. Meanwhile, when a cargo is attached on a fuselage of a general multi-rotor, it can be described as when the condition $\mathbf{q}_T = \mathbf{q}_F$ is satisfied during the entire flight. Applying the above constraint in equation (10), the rotational dynamics of T^3-Multirotor becomes as follows

$$(J_T + J_F)\ddot{\mathbf{q}}_T = \mathbf{T}_T,\ \mathbf{q}_T = \mathbf{q}_F \quad (13)$$

which requires additional torque of $J_F\ddot{\mathbf{q}}_T$ for the multi-rotor to exhibit the same behavior as in slung-load transportation.

A. Relative Attitude Control (RAC) Strategy: Fixing $\mathbf{q}_F$ by adequate servomechanism control

As an eclectic solution to the above two situations, we propose a method of fixing the value of $\mathbf{q}_F$ during the flight among the various parameters of T^3-Multirotor. For the convenience of analysis, we assume that the platform is in the horizontal motion and maintains the constant heading angle of $\psi_T = 0$.

Consider the situation where $\phi_F = 0,\ \theta_F = 0$ is already achieved with proper $\mathbf{T}_{T\to F}$ control. At this time, ψ_F always has the same value as ψ_T, which is zero, due to the characteristics of the universal joint. Then, the relative attitude control torque $\mathbf{T}_{T\to F}$ for keeping $\mathbf{q}_F = [0\ 0\ 0]^T$ is calculated based on equation (10) as

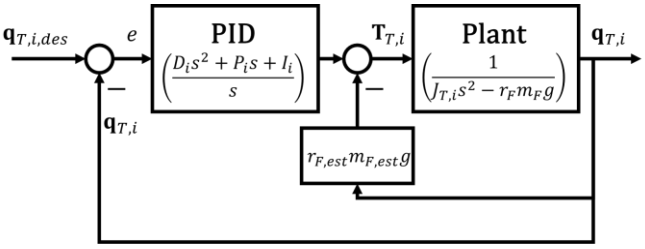

Figure 5. Attitude control algorithm of T^3-Multirotor with proposed strategy.

$$\mathbf{T}_{T\to F} = -\left(\frac{m_F}{M}\right) r_F F_T \begin{bmatrix} s\phi_T \\ c\phi_T s\theta_T \\ 0\end{bmatrix}, \quad (14)$$

where $\mathbf{r}_F = [0\ 0\ -r_F]^T, r_F \in \mathbb{R} \geq 0$. The symbols $s(*)$ and $c(*)$ refer to sine and cosine functions, respectively. If the platform is in level flight, then $\ddot{z}_T$ should be zero. With equations (6) and (7), F_T for satisfying $\ddot{z}_T = 0$ is calculated as

$$F_T = \frac{Mg}{c\phi_T c\theta_T}, \quad (15)$$

and $\mathbf{T}_{T\to F}$ for horizontal flight becomes as follows

$$\mathbf{T}_{T\to F} = -r_F m_F g \begin{bmatrix} \frac{t\phi_T}{c\theta_T} \\ t\theta_T \\ 0\end{bmatrix}, \quad (16)$$

where $t(*)$ refers the tangent function. When we apply the small angle assumption to induce the simplified final form, the rotational equations of motion of the T^3-Multirotor in level flight becomes as follows.

$$\begin{cases} J_T\ddot{\mathbf{q}}_T \approx \mathbf{T}_T + r_F m_F g \mathbf{q}_T \\ J_F\ddot{\mathbf{q}}_F \approx [0\ 0\ 0]^T \end{cases} \quad (17)$$

From the results of equation (17), we can see that the TGP with proposed strategy behaves similarly to the multi-rotor with only J_T of MOI, but generates additional torque of $r_F m_F g \mathbf{q}_T$ which changes in magnitude according to the current attitude. The transfer function that expresses the relationship between $\mathbf{T}_T$ and $\mathbf{q}_T$ then becomes as follows

$$\frac{\mathbf{q}_{T,i}(s)}{\mathbf{T}_{T,i}(s)} \approx \frac{1}{J_{T,i}s^2 - r_F m_F g}, i = 1,2, \quad (18)$$

where $i = 1,2$ represent x and y axis. From the transfer function, we can see that the system is an unstable system containing right half plane pole. In order to overcome the instability problem, we designed the attitude controller as shown in **Figure 5**. Then, the overall transfer function $\mathbf{\Gamma}_i(s)$ that represents the relationship between $\mathbf{q}_{T,i,des}$ and $\mathbf{q}_{T,i}$ becomes as

$$\mathbf{\Gamma}_i = \frac{\mathbf{q}_{T,i}}{\mathbf{q}_{T,i,des}} \approx \frac{D_{TGP,i}s^2 + P_{TGP,i}s + I_{TGP,i}}{J_{T,i}s^3 + D_{TGP,i}s^2 + (P_{TGP,i} + (r_{F,est}m_{F,est} - r_F m_F)g)s + I_{TGP,i}}, \quad (19)$$

where $P_{TGP,i}$, $I_{TGP,i}$, and $D_{TGP,i}$ are controller gains of TGP attitude controller, $r_{F,est}$ and $m_{F,est}$ are variables that need to be adjusted similar to the actual r_F and m_F values. When the values of $r_{F,est}$ and $m_{F,est}$ are appropriately tuned or measured, we can expect the system to behave similar to a multi-rotor with MOI only for J_T.

B. Relative Attitude Controller Design

Since the constant attitude control performance of the TGP irrespective of the size of J_F requires an $\mathbf{q}_F \approx 0$ assumption, we need to design a servomechanism controller that achieves this goal. The T^3-Multirotor can measure the attitude of the TGP from the inertial measurement unit (IMU) sensor attached to the TGP and measure the relative attitude $\theta_{rr} = \phi_T - \phi_F$ and $\theta_{rp} = \theta_T - \theta_F$ through the encoders attached to the servo motor. This allows us to construct an independently operating relative attitude controller with $\theta_{rr,des} = \phi_T$, $\theta_{rp,des} = \theta_T$ as target relative attitudes.

First, let us construct a simplified dynamic equation for the attitude of TGP and FP. If we apply equation (16) after applying the small angle assumption to equation (12), the simplified attitude dynamics of TGP and FP become as follows.

$$\begin{cases} \ddot{\phi}_T \approx J_{1,T}^{-1}(\tau_{r,T} + \tau_{s,r}) \\ \ddot{\theta}_T \approx J_{2,T}^{-1}(\tau_{p,T} - \tau_{s,p}) \end{cases} \tag{20}$$

$$\begin{cases} \ddot{\phi}_F \approx J_{1,F}^{-1}(m_F r_F g \phi_T - \tau_{s,r}) \\ \ddot{\theta}_F \approx J_{2,F}^{-1}(m_F r_F g \theta_T + \tau_{s,p}) \end{cases} \tag{21}$$

From equation (21), we can find the transfer function between TGP and FP attitude. If we apply the PID controller for servomechanism as

$$\begin{cases} \tau_{s,r} = \frac{D_{servo,1}s^2 + P_{servo,1}s + I_{servo,1}}{s}(\theta_{rr} - \theta_{rr,des}) \\ \tau_{s,p} = -\frac{D_{servo,2}s^2 + P_{servo,2}s + I_{servo,2}}{s}(\theta_{rp} - \theta_{rp,des}), \end{cases} \tag{22}$$

the transfer function between TGP attitude and the FP attitude becomes as

$$\begin{cases} \frac{\phi_F(s)}{\phi_T(s)} = \frac{m_F r_F g s}{J_{1,F}s^3 + D_{servo,1}s^2 + P_{servo,1}s + I_{servo,1}} \\ \frac{\theta_F(s)}{\theta_F(s)} = \frac{m_F r_F g s}{J_{2,F}s^3 + D_{servo,2}s^2 + P_{servo,2}s + I_{servo,2}}. \end{cases} \tag{23}$$

From equation (23), we can secure the performance of the servomechanism that keeps $\mathbf{q}_F$ at zero attitude by finding the maximum gain of the transfer function throughout the entire frequency range. Also, the stability of the relative attitude control system according to the operation of the servomechanism can be analyzed by obtaining the pole position of the transfer function.

C. Range of Physical Quantities of FP for the Benefit of the Proposed Strategy

The objective of this research is to enable stable attitude control through RAC when cargo is attached to the body. As mentioned above, the reason why the sling load transportation or the proposed technique is advantageous for stable attitude control compared to the conventional multi-rotor transportation method is that the posture is not controlled together with the cargo. In order to maintain this advantage, it is necessary that the maximum value of the attitude-controlling torque generated during the flight using the T^3 -Multirotor should be smaller than the value generated during the flight using the general multi-rotor. Now, let us find the range of $r_F m_F g$ that ensures smaller maximum required attitude-controlling torque compared to the general multi-rotor with equation (13), while the magnitude of the maximum required attitude-controlling torque does not exceed the maximum possible attitude-controlling torque in present platform mass condition. Since the dynamics of the roll and pitch motion of the multi-rotor is the same, the analysis is performed based on the roll motion.

1) Inequality equation: Let $\ddot{\phi}_{max}$ be the maximum roll angular acceleration, and ϕ_{max} be the maximum roll attitude of the conventional multi-rotor during the flight. In the case of conventional multi-rotor, the maximum attitude-controlling torque $M_{r,c}$ during flight is calculated based on equation (13) as

$$M_{r,c} = (J_{1,T} + J_{1,F})\ddot{\phi}_{max}. \tag{24}$$

Meanwhile, the maximum attitude-controlling torque $M_{r,t}$ during flight is calculated based on equation (17) as

$$M_{r,t} = J_{1,T}\ddot{\phi}_{max} + r_F m_F g \phi_{max}. \tag{25}$$

In order to obtain the advantage of T^3-Multirotor, $M_{r,c} \geq M_{r,t}$ must be satisfied. Accordingly, the range of the $r_F m_F g$ is as follows.

$$r_F m_F g \leq \frac{J_{1,F}\ddot{\phi}_{max}}{\phi_{max}} \tag{26}$$

Of the components on the right side of the inequality in equation (26), the ϕ_{max} value is generally given in the form of maximum attitude constraints while designing the attitude controller. However, the $\ddot{\phi}_{max}$ value is not given but determined by the dynamics of the multi-rotor and the maximum thrust force of the individual motor. Therefore, we need to find the value of $\ddot{\phi}_{max}$ to complete equation (26).

2) Calculation of $\ddot{\phi}_{max}$: The relationship between control input $u = [\mathbf{T}_T\ F_T]^T \in \mathbb{R}^{4\times1}$ and the motor force vector $\mathbf{F}_m = [F_1\ F_2\ F_3\ F_4]^T \in \mathbb{R}^{4\times1}$ of the multi-rotor is well known as follows [8]

$$u = B\mathbf{F}_m = \begin{bmatrix} 0 & r_a & 0 & -r_a \\ r_a & 0 & -r_a & 0 \\ b/k & -b/k & b/k & -b/k \\ 1 & 1 & 1 & 1 \end{bmatrix} \mathbf{F}_m \tag{27}$$

where $r_a \in \mathbb{R}$ represents the motor arm length, $b \in \mathbb{R}$ and $k \in \mathbb{R}$ represents reaction torque constant and force constant, respectively. Then, the required $\mathbf{F}_m$ during level flight is obtained from equations (15) and (27) as follows

$$\mathbf{F}_m = \begin{bmatrix} F_1 \\ F_2 \\ F_3 \\ F_4 \end{bmatrix} = B^{-1} \begin{bmatrix} \tau_{r,T} \\ \tau_{p,T} \\ 0 \\ \frac{Mg}{c\phi_T c\theta_T} \end{bmatrix} = \begin{bmatrix} \frac{1}{4}\frac{Mg}{c\phi_T c\theta_T} + \frac{1}{2r_a}\tau_{p,T} \\ \frac{1}{4}\frac{Mg}{c\phi_T c\theta_T} + \frac{1}{2r_a}\tau_{r,T} \\ \frac{1}{4}\frac{Mg}{c\phi_T c\theta_T} - \frac{1}{2r_a}\tau_{p,T} \\ \frac{1}{4}\frac{Mg}{c\phi_T c\theta_T} - \frac{1}{2r_a}\tau_{r,T} \end{bmatrix}, \quad (28)$$

where $\tau_{y,T} = 0$ due to our fixed heading angle assumption. If we set the maximum force of the motor as F_{max}, then the range of possible roll-controlling torque is as follows.

$$|\tau_{r,T}| \le \tau_{T,max} = 2r_a \left(F_{max} - \frac{1}{4}\frac{Mg}{c\phi_{max} c\theta_{max}}\right) \quad (29)$$

Since we can achieve the maximum attitude-controlling torque through equation (29), we can calculate $\ddot{\phi}_{max}$ with equation (25) as

$$\ddot{\phi}_{max} = \frac{1}{J_{1,T}}(\tau_{T,max} - r_F m_F g \phi_{max}). \quad (30)$$

Through equations (26) and (30), the final form of $r_F m_F g$ inequality equation becomes as

$$r_F m_F g \le \frac{J_{1,F}}{(J_{1,T}+J_{1,F})\phi_{max}} \tau_{T,max}. \quad (31)$$

Thus, we can see that if the T^3-Multirotor, which attaches the cargo/parcel on the FP, holds $\mathbf{q}_F = 0$ through the servomechanism and satisfies the condition of equation (31), the maximum required attitude-controlling torque is always lower than that of the conventional multi-rotor with a guarantee of not exceeding the maximum possible attitude-controlling torque of present platform mass condition.

5. EXPERIMENTAL RESULT

A. Attitude Control Performance of TGP

In order to verify the performance of the T^3-Multirotor using the proposed relative attitude control strategy, an experiment is carried out with a platform carrying a box-type cargo at an indoor flight arena with a VICON motion capture system. The physical quantities including the cargo of the T^3-Multirotor used in the experiment are shown in Table 1. Based on the inequality condition of equation (23), the value of $r_F m_F g$ should not exceed 2.3096. However, the value of $r_F m_F g$ of T^3-Multirotor is 1.89, so that the payload-added platform used in this experiment does not exceed more than a maximum torque and requires less torque than the conventional multi-rotor.

In **Figure 6**, the graphs in the left column show the result of the attitude control with the same PID controller without changing the control method in RAC-on situation. Meanwhile, the graphs in the right column show the result of applying the control scheme proposed in **Figure 4** in the RAC-on situation. The red bold lines are the flight log that indicates whether the RAC is on or off, where the red line with the value of -0.5 indicates RAC-off situation and the value of +0.5 indicates RAC-on situation.

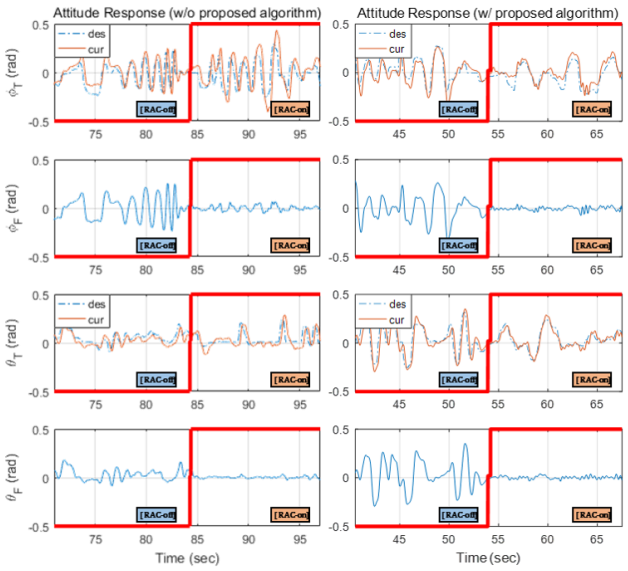

Figure 6. Attitude control performance of TGP and FP before (left column) and after (right column) applying proposed TGP attitude control technique.

In both cases, the attitude of the FP is kept at a value not exceeding ± 0.05 rad throughout the flight when the RAC is turned on, due to the well-behaving servomechanism that operates independently from TGP attitude control algorithm. However, the left graph shows that the posture control overshoots in the RAC-on situation when proposed TGP control algorithm is not applied. This result is due to the additional torque component that occurs as a reaction by the motion of the FP that is transmitted to the TGP through the universal joint, as expected in equation (18) for the RAC-off case. On the other hand, the results of the right column graph using the proposed TGP control algorithm show that the attitude control is smooth even in the RAC-on situation.

Table 1. THE PHYSICAL QUANTITIES OF THE T^3-MULTIROTOR USED IN THE EXPERIMENT

Name	Value	Name	Value
$J_{T,i}$	0.018 kg·m^2	m_T	1 Kg
$J_{F,i}$	0.040 kg·m^2	m_F	2.7 Kg
r_T	0.03 m	r_F	0.07 m
ϕ_{max}	0.3 rad	F_{max}	16 N
r_a	0.275 m		

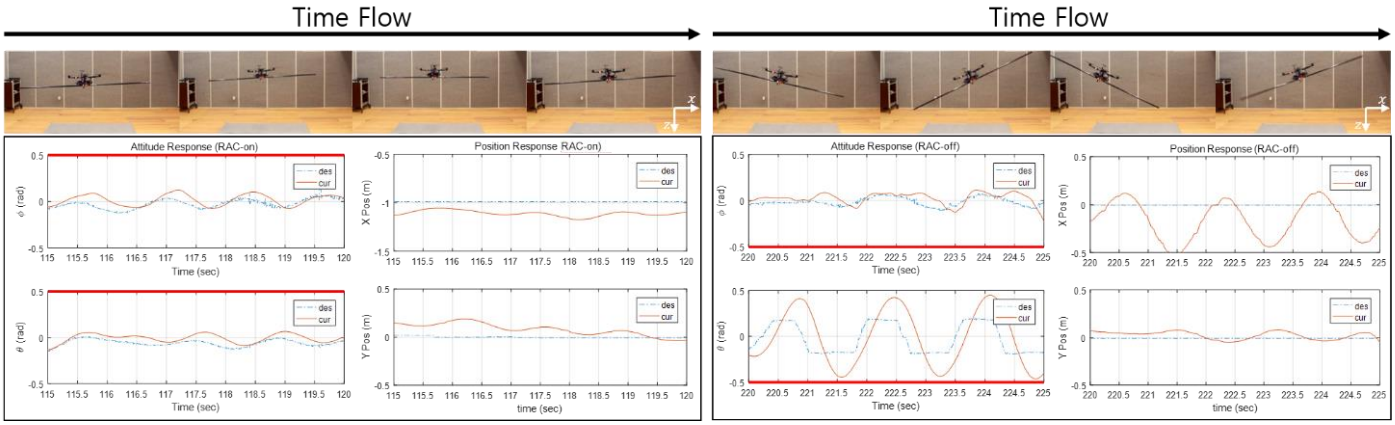

Figure 7. Results of hovering flight with (left) and without (right) relative attitude control (RAC) algorithm.

B. Verification of High-MOI Freight transportation Capability

In order to validate the flight performance under extreme condition, a rod-shaped cargo with a length of 2 m is attached to the FP. At this time, the rod is attached perpendicular to the pitch axis of the FP, therefore the MOI with respect to the pitch axis of the FP is greatly increased. The goal of the proposed technique is to keep the roll and pitch attitude of the FP always zero by utilizing the servomechanism and set the TGP which generates the propulsion necessary for the flight to be independent of the FP.

Figure 7 shows the comparison of flight performance with or without the use of the proposed RAC technique in the hovering flight of a multirotor with rod-shaped cargo attachment. The left set of figures show the result of the proposed method and those on the right show the result of flying with the relative attitude between TGP and FP fixed at zero. In both cases, the same TGP attitude controller was applied. Due to our heading angle setting of this experiment, the rolling motion of the multirotor governs the Y-direction position movement and the pitching motion governs the X-direction position movement. The 'TGP Attitude Response' graph of each figure set shows the desired and current attitude of the TGP, and the 'FP Attitude Response' graph shows the current attitude of the FP part. When RAC is not applied, the attitude of TGP and FP are the same, but when RAC is applied, the roll and pitch attitude of FP is always controlled to be zero. The 'Position Response' graph shows the desired and current position of the aircraft. Both flights are set to hover at the designated location in the three-dimensional space. In the case of the flight with RAC applied, we can see that the attitude and position control performance are satisfactory compared with the case where RAC is not applied. On the other hand, in the case of the flight without RAC applied, a serious decline in the attitude control performance is observed in pitch attitude motion in which the MOI of the fuselage in pitch axis is greatly increased due to the attachment of the rod-shaped cargo. As a result of the degradation in attitude control performance, we can see that the position control performance in the X-direction is also drastically decreased.

6. CONCLUSION

In this paper, we introduced a freight transport technique using a T^3-Multirotor free from the pendulum movement of cargo, which can cause control instability while taking advantage of sling road freight transportation which can control the cargo independently of cargo. Through the relative attitude control between TGP and FP, which is a unique capability of T^3-Multirotor, the cargo attitude $\mathbf{q}_F$ can be kept at zero all the time during the flight. In addition, we analyzed the motion characteristics in RAC-on situation that is different from general multi-rotors, and introduced a control strategy to overcome the deterioration of control performance.

Through this study, we expect to be able to carry freight freely from the constraints of sling-load cargo transportation technique, even in an outdoor environment that has no motion capture system to measure the swing angle, or climatic disturbance environment that can cause unpredictable pendulum movement.

APPENDIX

A. Relationship between θ_{rs} and θ_{rr}

$$f_r(\theta_{rs}) = \operatorname{acos}\left(\frac{r_{fa}^2+k_r^2-r_{rr}^2}{2r_{fa}k_r}\right) - \operatorname{asin}\left(\frac{r_{rh}}{k_r}\sin(\theta_{r2}-\theta_{rs})\right) - \theta_{r2}$$
$$k_r = \sqrt{r_{tj}^2+r_{rh}^2-2r_{tj}r_{rh}\cos(\theta_{r2}-\theta_{rs})}$$
$$\theta_{r1} = \operatorname{atan}\left(\frac{r_{ts}}{r_{tu}}\right),\ \theta_{r2} = \frac{\pi}{2}-\theta_{r1},\ r_{tj} = \sqrt{r_{tu}^2+r_{ts}^2}$$

B. Relationship between θ_{ps} and θ_{rp}

$$f_p(\theta_{ps}) = \frac{\pi}{2} - \operatorname{acos}\left(\frac{r_{ta}^2+k_p^2-r_{pr}^2}{2r_{ta}k_p}\right) - \operatorname{asin}\left(\frac{r_{ph}}{k_p}\sin(\theta_{p2}+\theta_{ps})\right) - \theta_{p1}$$
$$k_p = \sqrt{r_{fj}^2+r_{ph}^2+2r_{fj}r_{ph}\cos(\theta_{p2}+\theta_{ps})}$$
$$\theta_{p1} = \operatorname{atan}\left(\frac{r_{fs}}{r_{fu}}\right),\ \theta_{p2} = \frac{\pi}{2}-\theta_{p1},\ r_{fj} = \sqrt{r_{fu}^2+r_{fs}^2}$$

REFERENCES

[1] Goodarzi, Farhad A., Daewon Lee, and Taeyoung Lee. "Geometric stabilization of a quadrotor UAV with a payload

connected by flexible cable." American Control Conference (ACC), 2014. IEEE, 2014.
[2] Sadr, Sara, S. Ali A. Moosavian, and Payam Zarafshan. "Dynamics modeling and control of a quadrotor with swing load." Journal of Robotics 2014 (2014).
[3] Lee, Seung Jae, Jaehyun Yoo, and H. Jin Kim. "Design, Modeling and Control of T3-Multirotor: A Tilting Thruster Type Multirotor" 2018 IEEE International Conference on Robotics and Automation (ICRA). IEEE, 2018.
[4] Bisgaard, Morten. Modeling, estimation, and control of helicopter slung load system. Department of Control Engineering, Aalborg University, 2008.
[5] Vargas, Aldo, Murray L. Ireland, and David Anderson. "Swing-Free Manoeuvre Controller for Rotorcraft Unmanned Aerial Vehicle Slung-Load System Using Echo State Networks." International Journal of Unmanned Systems Engineering. 3.1 (2015): 26.
[6] Goodarzi, Farhad A., Daewon Lee, and Taeyoung Lee. "Geometric stabilization of a quadrotor UAV with a payload connected by flexible cable." American Control Conference (ACC), 2014. IEEE, 2014.
[7] Lee, Seung Jae, and H. Jin Kim. "Autonomous swing-angle estimation for stable slung-load flight of multi-rotor UAVs." Robotics and Automation (ICRA), 2017 IEEE International Conference on. IEEE, 2017.
[8] Beard, Randal. "Quadrotor dynamics and control rev 0.1." (2008).